

## RECONSIDERATION OF THE CRYSTAL STRUCTURE OF PARANATISITE AND THE CRYSTAL CHEMISTRY OF $[^{61}M_2 \ ^{41}T_2 \ \phi_{12}]$ SHEETS

ELENA SOKOLOVA<sup>§</sup> AND FRANK C. HAWTHORNE

Department of Geological Sciences, University of Manitoba, Winnipeg, Manitoba R3T 2N2, Canada

### ABSTRACT

The crystal structure of paranatisite, ideally  $\text{Na}_4 [\text{Ti O Ti O} (\text{SiO}_4)_2]$ , from the Khibina–Lovozero alkaline complex, Kola Peninsula, Russia,  $a$  9.181(2),  $b$  4.800(1),  $c$  9.811(2) Å,  $V$  432.37(1) Å<sup>3</sup> has been refined in the space group  $Pmc2_1$  ( $Z = 2$ ) to a residual  $R$  value of 5.1% using 651 observed ( $|F_o| > 4\sigma F$ ) reflections collected with a single-crystal diffractometer, a serial detector and  $\text{MoK}\alpha$  X-radiation. The empirical formula, space group and crystal chemistry of paranatisite are revised. There is one unique  $Si$  tetrahedron, three unique  $Na$  octahedra and two unique  $Ti$  square pyramids with  $\langle Si-O \rangle = 1.629$ ,  $\langle Na-O \rangle = 2.430$  and  $\langle Ti-O \rangle = 1.971$  Å. The crystal structure of paranatisite is described in terms of seven polyhedral layers, with emphasis on the role of three types of sheets. Two sheets consist of  $(\text{TiO}_5)$  square pyramids,  $(\text{SiO}_4)$  tetrahedra and  $(\text{NaO}_6)$  octahedra; the third sheet consists of  $(\text{NaO}_6)$  octahedra and  $(\text{SiO}_4)$  tetrahedra. These sheets are based on the  $4^4$  plane net in which the vertices are colored to represent occupancy by different cations and vacancies ( $\square$ ). A sheet can be characterized by the unit  $[^{61}M_2 \ ^{41}T_2 \ \phi_{12}]$ , where  $M$  generally represents [6]- or [5]-coordinated cations,  $T$  represents [4]-coordinated cations,  $\phi$  stands for an anion (O, F, Cl, OH, H<sub>2</sub>O), and  $(M\phi_n)$  and  $(\text{TO}_4)$  polyhedra share common vertices. This sheet occurs as a component in the structures of several minerals: sulphohalite,  $\text{Na}_6 [(\text{SO}_4)_2] \text{F Cl}$ ; natisite,  $\text{Na}_2 [\text{Ti O} (\text{SiO}_4)]$ ; garnet,  $[^{81}M_3 \ ^{61}M_2 \ T_3 \ O_{12}]$ ; graphite,  $(\text{Mn}^{2+}, \text{Ca}, \text{Na}, \text{Li})_{24} \text{Ca}_4 \text{Fe}^{2+}_4 \text{Al}_8 (\text{PO}_4)_{24} \text{F}_8$ ; girvasite,  $\text{Na Ca}_2 [\text{Mg}_3 (\text{OH})_2 (\text{PO}_4)_2 \{ \text{PO}_2 (\text{OH})_2 \} (\text{H}_2\text{O})_4]$ ; olmsteadite,  $\text{K}_2 [\text{Fe}^{2+}_4 \text{Nb}_2 \text{O}_4 (\text{H}_2\text{O})_4]$ ; gainesite,  $\text{Na}_2 [\text{Zr}_2 \text{Be} (\text{PO}_4)_4]$ ; rhomboclase,  $(\text{H}_5\text{O}_2) [\text{Fe} (\text{SO}_4)_2 (\text{H}_2\text{O})_2]$ ; and several uranium minerals related to meta-autunite,  $\text{Ca} [(\text{UO}_2) (\text{PO}_4)]_2 (\text{H}_2\text{O})_6$ .

**Keywords:** paranatisite, crystal structure, Khibina–Lovozero complex, crystal chemistry,  $4^4$  net, mixed  $M$ – $T$  sheet.

### SOMMAIRE

Nous avons affiné la structure cristalline de la paranatisite, de formule idéale  $\text{Na}_4 [\text{Ti O Ti O} (\text{SiO}_4)_2]$ , provenant du complexe alcalin de Khibina–Lovozero, péninsule de Kola, en Russie,  $a$  9.181(2),  $b$  4.800(1),  $c$  9.811(2) Å,  $V$  432.37(1) Å<sup>3</sup>, groupe spatial  $Pmc2_1$  ( $Z = 2$ ) jusqu'à un résidu  $R$  de 5.1% en utilisant 651 réflexions observées ( $|F_o| > 4\sigma F$ ) prélevées sur cristal unique avec un diffractomètre muni d'un détecteur en série et un rayonnement  $\text{MoK}\alpha$ . La formule empirique, le groupe spatial et la cristallographie de la paranatisite sont révisés. Il y a un tétraèdre  $Si$  unique, trois octaèdres  $Na$  uniques, et deux pyramides carrées  $Ti$ , avec  $\langle Si-O \rangle = 1.629$ ,  $\langle Na-O \rangle = 2.430$  et  $\langle Ti-O \rangle = 1.971$  Å. Nous décrivons la structure de la paranatisite en termes de sept feuillets de polyèdres, avec emphase sur le rôle de trois sortes de feuillets. Deux de ces feuillets sont faits de pyramides carrées  $(\text{TiO}_5)$ , des tétraèdres  $(\text{SiO}_4)$  et des octaèdres  $(\text{NaO}_6)$ ; le troisième feuillet contient des octaèdres  $(\text{NaO}_6)$  et des tétraèdres  $(\text{SiO}_4)$ . Ces feuillets sont fondés sur un réseau  $4^4$  en plan dans lequel les noeuds sont colorés pour représenter l'occupation des divers cations et des lacunes ( $\square$ ). Un feuillet peut se caractériser par l'expression  $[^{61}M_2 \ ^{41}T_2 \ \phi_{12}]$ , dans laquelle  $M$  représenterait en général des cations à coordinence [6] ou [5],  $T$  représente des cations à coordinence [4],  $\phi$  représente un anion (O, F, Cl, OH, H<sub>2</sub>O), et les polyèdres  $(M\phi_n)$  et  $(\text{TO}_4)$  partagent des coins communs. Un tel feuillet se trouve aussi dans la structure de plusieurs minéraux: sulphohalite,  $\text{Na}_6 [(\text{SO}_4)_2] \text{F Cl}$ ; natisite,  $\text{Na}_2 [\text{Ti O} (\text{SiO}_4)]$ ; grenat,  $[^{81}M_3 \ ^{61}M_2 \ T_3 \ O_{12}]$ ; graphite,  $(\text{Mn}^{2+}, \text{Ca}, \text{Na}, \text{Li})_{24} \text{Ca}_4 \text{Fe}^{2+}_4 \text{Al}_8 (\text{PO}_4)_{24} \text{F}_8$ ; girvasite,  $\text{Na Ca}_2 [\text{Mg}_3 (\text{OH})_2 (\text{PO}_4)_2 \{ \text{PO}_2 (\text{OH})_2 \} (\text{H}_2\text{O})_4]$ ; olmsteadite,  $\text{K}_2 [\text{Fe}^{2+}_4 \text{Nb}_2 \text{O}_4 (\text{H}_2\text{O})_4]$ ; gainesite,  $\text{Na}_2 [\text{Zr}_2 \text{Be} (\text{PO}_4)_4]$ ; rhomboclase,  $(\text{H}_5\text{O}_2) [\text{Fe} (\text{SO}_4)_2 (\text{H}_2\text{O})_2]$ ; et plusieurs minéraux d'uranium apparentés à la méta-autunite,  $\text{Ca} [(\text{UO}_2) (\text{PO}_4)]_2 (\text{H}_2\text{O})_6$ .

**Mots-clés:** paranatisite, structure cristalline, complexe de Khibina–Lovozero, cristallographie, réseau  $4^4$ , feuillet  $M$ – $T$  mixte.

<sup>§</sup> E-mail address: sokolova@ms.umanitoba.ca

## INTRODUCTION

Paranatisite, ideally  $\text{Na}_2 [\text{Ti O} (\text{SiO}_4)]$ , has been described from hyperagpaitic pegmatitic rocks of the Khibina–Lovozero alkaline complex, Kola Peninsula, Russia (Khomyakov *et al.* 1992). Sokolova *et al.* (1985) showed that paranatisite is a low-temperature orthorhombic modification of natisite,  $\text{Na}_2 [\text{Ti O} (\text{SiO}_4)]$ , tetragonal (Nyman *et al.* 1978). Polymorphism is typical of zirconosilicates occurring in hyperalkaline rocks, *e.g.*, catapleite,  $\text{Na}_2 \text{Zr Si}_3 \text{O}_9 (\text{H}_2\text{O})_2$  (Ilyushin *et al.* 1981b) and gaidonnayite,  $\text{Na}_2 \text{Zr Si}_3 \text{O}_9 (\text{H}_2\text{O})_2$  (Chao 1985); umbite,  $\text{K}_2 \text{Zr Si}_3 \text{O}_9 (\text{H}_2\text{O})$  (Ilyushin 1993) and kostylevite,  $\text{K}_4 \text{Zr}_2 \text{Si}_6 \text{O}_{18} (\text{H}_2\text{O})_2$  (Ilyushin *et al.* 1981a). When describing the crystal structure of paranatisite, Sokolova *et al.* (1985) used an average-structure model, neglecting disorder of oxygen atoms; the resulting configuration of anions is rather unsatisfactory. Consequently, we have re-examined the structure of paranatisite. Here, we present results of our refinement of the paranatisite structure and describe it in terms of seven layers of polyhedra, including three types of  $[\text{M}_2^{[6]} \text{T}_2^{[4]} \phi_{12}]$  sheets. We also examine some

topologically related structures: sulphohalite,  $\text{Na}_6 [(\text{SO}_4)_2] \text{F Cl}$ ; natisite,  $\text{Na}_2 [\text{Ti O} (\text{SiO}_4)]$ ; garnet,  $[\text{M}_3^{[8]} \text{M}_2 \text{T}_3 \text{O}_{12}]$ ; graphite,  $(\text{Mn}^{2+}, \text{Ca}, \text{Na}, \text{Li})_{24} \text{Ca}_4 \text{Fe}^{2+}_4 \text{Al}_8 (\text{PO}_4)_{24} \text{F}_8$ ; girvasite,  $\text{Na Ca}_2 [\text{Mg}_3 (\text{OH})_2 (\text{PO}_4)_2 \{ \text{PO}_2 (\text{OH})_2 \} (\text{CO}_3) (\text{H}_2\text{O})_4]$ ; olmsteadite,  $\text{K}_2 [\text{Fe}^{2+}_4 \text{Nb}_2 \text{O}_4 (\text{H}_2\text{O})_4 (\text{PO}_4)_4]$ ; rhomboclase,  $(\text{H}_5\text{O}_2) [\text{Fe} (\text{SO}_4)_2 (\text{H}_2\text{O})_2]$ ; gainesite,  $\text{Na}_2 [\text{Zr}_2 \text{Be} (\text{PO}_4)_4]$ , and several uranium minerals related to meta-autunite,  $\text{Ca} [(\text{UO}_2) (\text{PO}_4)]_2 (\text{H}_2\text{O})_6$ , that contain the topologically identical sheet  $[\text{M}_2^{[6]} \text{T}_2^{[4]} \phi_{12}]$ .

## EXPERIMENTAL

Crystals of paranatisite are yellow to orange-yellow, and transparent; they show mottled extinction in cross-polarized light. A relatively optically homogeneous crystal of paranatisite from the holotype specimen was attached to a glass fiber and mounted on a Siemens P4 automated four-circle diffractometer. Reflections over the range  $9.4 \leq 2\theta \leq 29.4^\circ$  were centered, and the unit-cell dimensions were refined by least squares from the resultant setting angles. A small number of those reflections that were centered did not fit the refined cell very well, and the standard deviations of this refined cell were large. When these reflections were omitted from the refinement, the remainder of the data fit the cell given in Table 2. It should be noted that the crystal quality is poor, and there were problems centering on some reflections. Intensity data were collected in  $\theta$ - $2\theta$  scan mode at a fixed scan-rate of  $2.0^\circ/2\theta/\text{min}$ ; a total of 1402 intensities was measured. Psi-scan data were measured on 15 reflections to  $60^\circ 2\theta$  at increments of  $5^\circ$ , and an absorption correction, modeling the crystal as a triaxial ellipsoid, reduced  $R(\text{azimuthal})$  from 9.1 to 3.9%. The data were corrected for Lorentz, polarization and background effects, averaged and reduced to structure factors; of the 705 unique reflections, 651 were considered as observed ( $|F_o| > 4\sigma F$ ).

TABLE 1. MISCELLANEOUS INFORMATION FOR PARANATISITE

a (Å)	9.181(2)	radiation	MoK $\alpha$
b	4.800(1)	2 $\theta$ -range for data collection (°)	4–60
c	9.811(2)	R(int) (%)	4.5
V (Å <sup>3</sup> )	432.37(1)	Reflections collected	1402
Sp. Gr.	<i>Pmc</i> 2 <sub>1</sub>	Unique reflections	705
Z	2	$F_o > 4\sigma F$	651
Absorption coefficient (mm <sup>-1</sup> )	2.70	Goodness of fit on $F^2$	1.304
F(000)	396.3	R(obs) (%)	5.1
crystal size (mm)	0.08 x 0.24 x 0.20	R(all data) (%)	5.5
Refinement method: least-squares on $F^2$ ; fixed weights = $1/\sigma(F)$		wR <sub>2</sub>	14.5
$R = \sum   F_o  -  F_c   / \sum  F_o $			
$wR_2 = \{ \sum [w(F_o^2 - F_c^2)]^2 / \sum [w(F_o^2)]^2 \}^{1/2}$			
where $w = 1 / [\sigma^2(F_o^2) + (aP)^2 + bP]$ , $P = [2F_c^2 + \max(F_o^2, c)] / 3$			

TABLE 2. FINAL ATOM PARAMETERS FOR PARANATISITE

	x	y	z	U <sub>11</sub>	U <sub>22</sub>	U <sub>33</sub>	U <sub>23</sub>	U <sub>13</sub>	U <sub>12</sub>	U <sub>eq</sub>
Ti(1)	0	0.0342(2)	0.4594(7)	0.0001(5)	0.0090(6)	0.0079(6)	0.0010(13)	0	0	0.0057(4)
Ti(2A)	½	0.5248(19)	0.1782(15)	0.000(2)	0.012(3)	0.025(8)	-0.005(3)	0	0	0.012(3)
Ti(2B)	½	0.4777(17)	0.2422(13)	0.004(2)	0.009(3)	0.005(5)	0.0010(24)	0	0	0.006(2)
Si(1)	0.24961(11)	-0.0004(6)	0.2095(8)	0.0000(6)	0.0103(6)	0.0091(6)	0.0000(4)	-0.0009(11)	0.0016(14)	0.0065(4)
Na(1)	-0.24955(19)	0.4965(4)	0.4614(11)	0.0065(10)	0.0146(10)	0.0148(11)	0.0008(16)	-0.0012(18)	0.0030(8)	0.0120(5)
Na(2)	0	0.498(2)	0.2138(14)	0.0167(14)	0.0180(14)	0.0151(18)	0.0060(12)	0	0	0.0166(8)
Na(3)	½	0.0926(7)	-0.0406(11)	0.0065(12)	0.0158(13)	0.0165(13)	-0.003(4)	0	0	0.0129(6)
O(1)	0.1461(5)	0.1443(14)	0.5934(10)	0.006(2)	0.014(4)	0.016(3)	0.003(3)	-0.002(2)	-0.003(3)	0.0119(13)
O(2)	0.6497(6)	0.7522(15)	0.2730(10)	0.007(2)	0.015(3)	0.016(3)	0.002(3)	0.001(2)	-0.002(2)	0.0124(13)
O(3)	0	-0.3202(11)	0.4622(14)	0.009(2)	0.014(2)	0.015(2)	-0.002(5)	0	0	0.0128(10)
O(4)	0.1469(5)	0.1452(14)	0.3229(9)	0.002(2)	0.017(3)	0.012(3)	0.0005(24)	0.005(2)	0.004(3)	0.0105(12)
O(5)	0.3511(5)	0.2394(14)	0.1396(10)	0.002(2)	0.009(3)	0.017(3)	-0.0005(25)	0.002(2)	-0.003(2)	0.0093(12)
O(6)	½	-0.3533(13)	0.0112(11)	0.003(2)	0.016(3)	0.025(3)	-0.0002(28)	0	0	0.0145(12)

## STRUCTURE REFINEMENT

The crystal structure of paranatisite,  $\text{Na}_2[\text{TiO}(\text{SiO}_4)]$ , was refined with the SHELXTL 5.1 software (Sheldrick 1997). Scattering factors for neutral atoms were taken from the International Tables for X-Ray Crystallography (Ibers & Hamilton 1974). The present X-ray-diffraction data are consistent with space groups  $Pmcm$  and  $Pmc2_1$ . Note that the refined structure is not consistent with the presence of a mirror plane orthogonal to the  $c$  axis (Fig. 1c). Details of the X-ray data collection and structure refinement are given in Table 1. The crystal structure of paranatisite was refined to an  $R$  index of 5.1% in the space group  $Pmc2_1$ . Two maxima of about  $15e$  were found  $\sim 0.65 \text{ \AA}$  apart in the difference-Fourier map, and included in the refinement as the sites  $Ti(2A)$  and  $Ti(2B)$  with the scattering curve of Ti. Final atom parameters are given in Table 2, selected interatomic distances are presented in Table 3, and a bond-valence analysis is shown in Table 4. A table of structure factors may be obtained from The Depository of Unpublished Data, CISTI, National Research Council, Ottawa, Ontario K1A 0S2, Canada.

## ELECTRON-MICROPROBE ANALYSIS

The same crystal used for collection of the single-crystal X-ray intensity data was mounted in a perspex disc, ground, polished and coated with carbon for chemical analysis using a Cameca SX-50 electron mi-

TABLE 3. SELECTED INTERATOMIC DISTANCES ( $\text{\AA}$ ) FOR PARANATISITE

$Ti(1)-O(1)$	$\times 2$	1.951(7)	$Ti(2B)-O(2)$	$\times 2$	1.928(8)
$Ti(1)-O(3)$		1.701(6)	$Ti(2B)-O(5)$	$\times 2$	2.047(9)
$Ti(1)-O(4)$	$\times 2$	<u>1.974(6)</u>	$Ti(2B)-O(6)$		<u>2.407(2)</u>
$\langle Ti(1)-O \rangle$		1.910	$\langle Ti(2B)-O \rangle$		2.071
$Ti(2A)-O(2)$	$\times 2$	1.99(1)	$Ti(2A)-Ti(2B)$		0.667(4)
$Ti(2A)-O(5)$	$\times 2$	1.972(7)			
$Ti(2A)-O(6)a$		<u>1.74(2)</u>			
$\langle Ti(2A)-O \rangle$		1.933			
$Na(1)-O(1)b$		2.332(9)	$Na(2)-O(1)f$	$\times 2$	2.48(1)
$Na(1)-O(2)c$		2.40(1)	$Na(2)-O(3)a$		2.59(2)
$Na(1)-O(3)a$		2.454(3)	$Na(2)-O(3)g$		2.61(2)
$Na(1)-O(4)b$		2.36(1)	$Na(2)-O(4)$	$\times 2$	<u>2.42(1)</u>
$Na(1)-O(5)d$		2.35(1)	$\langle Na(2)-O \rangle$		2.50
$Na(1)-O(6)e$		<u>2.449(4)</u>			
$\langle Na(1)-O \rangle$		2.39			
$Na(3)-O(2)h$	$\times 2$	2.41(1)	$Si-O(1)i$		1.636(8)
$Na(3)-O(5)$	$\times 2$	2.34(1)	$Si-O(2)j$		1.629(7)
$Na(3)-O(6)$	$\times 2$	2.200(8)	$Si-O(4)$		1.618(7)
$Na(3)-O(6)a$		<u>2.708(7)</u>	$Si-O(5)$		<u>1.632(7)</u>
$\langle Na(3)-O \rangle$		2.37	$\langle Si-O \rangle$		1.629

a:  $x, 1+y, z$ ; b:  $-x, y, z$ ; c:  $-1+x, y, z$ ; d:  $-x, 1-y, \frac{1}{2}+z$ ;  
e:  $-x, -y, \frac{1}{2}+z$ ; f:  $-x, 1-y, -\frac{1}{2}+z$ ; g:  $-x, -y, -\frac{1}{2}+z$ ;  
h:  $1-x, 1-y, -\frac{1}{2}+z$ ; i:  $x, -y, -\frac{1}{2}+z$ ; j:  $1-x, -1+y, z$ .

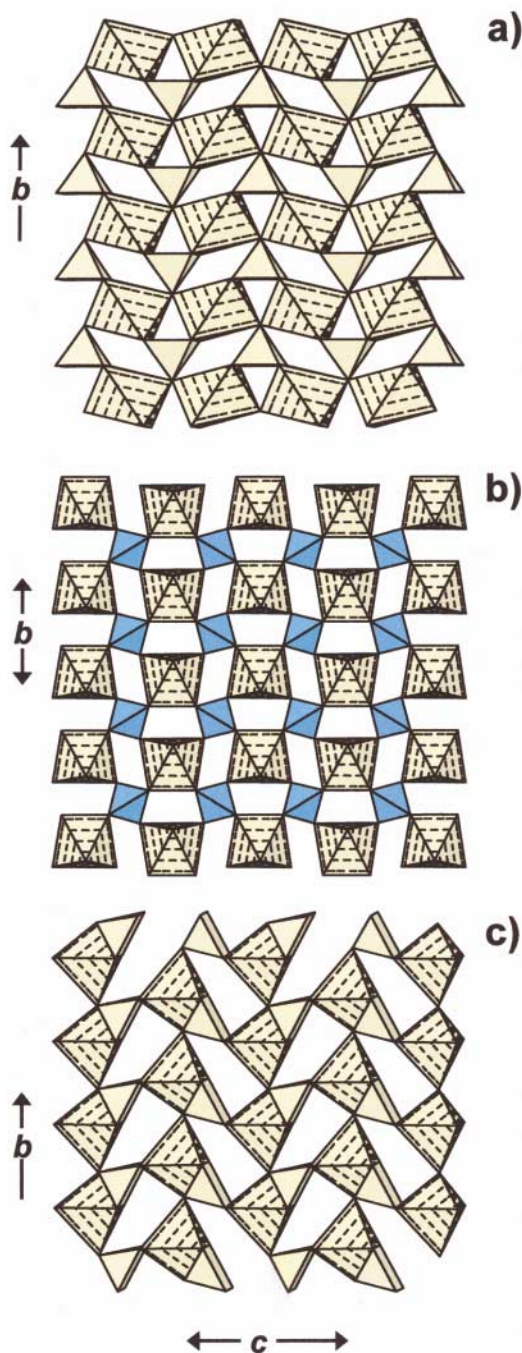


FIG. 1. Three (100) sheets in the crystal structure of paranatisite: (a) a sheet of [5]-coordinated  $Ti(1)$  polyhedra and  $Na(2)$  octahedra at  $x \approx 0$ ; (b) a sheet of  $Na(1)$  octahedra and  $Si$  tetrahedra at  $x \approx 0.25$ ; (c) a sheet of  $Na(3)$  octahedra and  $Ti(2)$  polyhedra at  $x \approx 0.5$ . The [5]-coordinated  $Ti$  polyhedra are yellow,  $Na$  octahedra are yellow (hachured), and  $Si$  tetrahedra are blue.

croprobe. The crystal was analyzed for Si, Ti, Zr, Nb, Ta, Fe, Ca, Na and F in wavelength-dispersion mode. Ten points were analyzed with the following conditions: excitation voltage: 15 kV, specimen current: 20 nA, beam size: 10  $\mu\text{m}$ , peak count-time: 20 s, background count-time: 10 s. The standards and crystals used for  $K\alpha$  X-ray lines of the elements sought were: Si: diopside; Mn: spessartine; Ti: titanite; Nb:  $\text{MnNb}_2\text{O}_6$ ; Fe: fayalite; Ca: diopside; Na: jadeite. The resulting chemical composition is given in Table 5; the unit formula was calculated on the basis of 10 O atoms, and is listed in Table 5.

#### CHEMICAL COMPOSITION

The chemical composition (Table 5) shows that paranatisite has significant Fe incorporated in the structure. Unfortunately, a combination of low Fe content and paucity of sample did not allow determination of the valence state of the Fe by milliprobe Mössbauer spectroscopy, and hence we must consider the possibility of both  $\text{Fe}^{3+}$  and  $\text{Fe}^{2+}$  in the structure of paranatisite. Again, the small amount of Fe present does not allow determination of valence state from differences in mean bond-lengths. We will thus consider two different possibilities: (1) all  $\text{Fe}^{3+}$ , and (2) all  $\text{Fe}^{2+}$ .

TABLE 4. BOND-VALENCE TABLE FOR PARANATISITE\*

	<i>Ti</i> (1)	<i>Ti</i> (2)**	Si	Na(1)	Na(2)	Na(3)	$\Sigma$
O(1)	0.67 <sup>2</sup>	1	0.98	0.23	0.18 <sup>2</sup>		2.06
O(2)		0.65 <sup>2</sup>	1.00	0.21		0.20 <sup>2</sup>	2.06
O(3)	1.36			0.19	0.15 0.14		1.84
O(4)	0.63 <sup>2</sup>	1	1.03	0.22	0.20 <sup>2</sup>		2.08
O(5)		0.57 <sup>2</sup>	0.93	0.23		0.23 <sup>2</sup>	1.96
O(6)		0.80		0.19 <sup>2</sup>		0.30 0.12	1.60
$\Sigma$	3.96	4.04	3.94	1.27	1.05	1.28	

\* Bond-valence curves (*vu*) from Brown (1981)

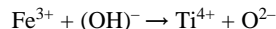
\*\* Calculated as the weighted mean for the *Ti*(2A) and *Ti*(2B) sites

TABLE 5. CHEMICAL COMPOSITION (wt.%)<sup>\*</sup> AND UNIT FORMULA (*apfu*) FOR PARANATISITE

$\text{SiO}_2$	29.24	Si	2.00
$\text{TiO}_2$	36.16		
$\text{Nb}_2\text{O}_5$	0.14	Ti	1.86
$\text{Fe}_2\text{O}_3$	4.69	$\text{Fe}^{3+}$	0.24
MnO	0.58	$\Sigma$	2.10
CaO	0.23		
$\text{Na}_2\text{O}$	<u>28.69</u>	Mn	0.04
$\Sigma$	99.73	Na	3.78
		Ca	<u>0.02</u>
		$\Sigma$	3.84

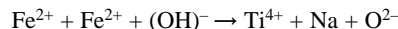
\* Ta, Zr, F not detected

For all  $\text{Fe}^{3+}$ , we presume that  $\text{Fe}^{3+}$  substitutes for  $\text{Ti}^{4+}$ . There are no other significant substitutions involving cations in natasite that can maintain electroneutrality, and hence there must be an accompanying anion-substitution of the form



Note that this type of substitution is in accord with the low incident bond-valence sum at the O(6) site, which would be partly occupied by  $\text{O}^{2-}$  and  $(\text{OH})^-$ , and may be the cause of the cation disorder at the *Ti*(2A) and *Ti*(2B) sites.

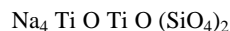
For all  $\text{Fe}^{2+}$ , we presume that half the  $\text{Fe}^{2+}$  substitutes for  $\text{Ti}^{4+}$  and the other half of the  $\text{Fe}^{2+}$  substitutes for Na at one or more of the *Na* sites. Again, there must be an accompanying anion substitution of the form



This substitution is also in accord with the low incident bond-valence sum at the O(6) site, and also may be the cause of cation disorder at the *Ti*(2A) and *Ti*(2B) sites.

Do the structural data allow us to decide between these two different models? No. Using the sum of the constituent cation and anion radii, the predicted  $\langle \text{Ti}(2\text{B})-\text{O} \rangle$  distances are 1.99 and 2.01 Å for  $\text{Fe}^{3+}$  and  $\text{Fe}^{2+}$ , respectively, whereas the observed  $\langle \text{Ti}(2\text{B})-\text{O} \rangle$  is 2.07 Å; the difference is too large to be indicative of valence state, and is probably the result of the extreme disorder in this part of the structure. The unit formula (Table 5) agrees somewhat better with the all- $\text{Fe}^{2+}$  alternative, but we do not regard this evidence as definitive, and the question of the valence state of Fe remains open.

The currently accepted structural formula of paranatisite,  $\text{Na}_2 [\text{Ti O} (\text{SiO}_4)]$ , is not very convenient, as there are two distinct *Ti* sites that can be occupied in the unit cell, *Ti*(1) and either *Ti*(2A) or *Ti*(2B), and these two sites behave differently. As shown below, *Ti*(1) is occupied by  $\text{Ti}^{4+}$  and *Ti*(2A,B) is occupied by  $\text{Ti}^{4+} + \text{Fe}^{3+}$ , and hence it is desirable to identify these two different sites in the structure formula. Moreover, there are six distinct O sites, five of which [O(1)–O(5)] are always occupied by  $\text{O}^{2-}$ , and the other of which [O(6)] is occupied by  $\text{O}^{2-}$  and  $(\text{OH})^-$ . We may identify these features by considering *Z* as 2 and writing the end-member formula as



The corresponding end-members for substitution of  $\text{Fe}^{3+}$  and  $\text{Fe}^{2+}$  at the *Ti*(2B) site are  $\text{Na}_4 \text{Ti O Fe}^{3+} (\text{OH}) (\text{SiO}_4)_2$  and  $(\text{Na}_3\text{Fe}^{2+}) \text{Ti O Fe}^{2+} (\text{OH}) (\text{SiO}_4)_2$ , respectively.

## STRUCTURE DESCRIPTION

*Coordination of the cations*

In the crystal structure of paranatisite, there is one unique *Si* site surrounded by four O atoms in a tetrahedral arrangement, with  $\langle Si-O \rangle = 1.629 \text{ \AA}$ . There are two unique [5]-coordinated *Ti* sites. The *Ti*(1) site has a  $\langle Ti(1)-O \rangle$  of  $1.910 \text{ \AA}$  and is fully occupied by Ti. The other *Ti* site involves positional disorder and was split into two sites, *Ti*(2A) and *Ti*(2B), with unconstrained occupancies of 0.54(4) and 0.46(4), respectively. The *Ti*(2A)–*Ti*(2B) distance is  $0.667(4) \text{ \AA}$ , indicating that only one of these sites can be occupied in any local arrangement. In accord with this, the (unconstrained) sum of the refined occupancies of the two sites is 1.00(5). The *Ti*(1) and *Ti*(2A) polyhedra can be described as square pyramids with four long bonds and one short bond:  $\langle Ti(1,2A)-O \rangle = 1.922$ ,  $Ti(1)-O(3) = 1.701$ ,  $Ti(2A)-O(6) = 1.74 \text{ \AA}$ , similar to [5]-coordinated Ti in the crystal structure of natisite,  $Na_2 [Ti O (SiO_4)]$  (Table 6):  $\langle Ti-O \rangle = 1.931$ ,  $Ti-O(2) = 1.695 \text{ \AA}$  (Nyman *et al.* 1978). The coordination of *Ti*(2B) in paranatisite is very different:  $\langle Ti(2B)-O \rangle = 2.071$ ,  $Ti(2B)-O(6) = 2.407 \text{ \AA}$ . For the *Ti* sites, we did not find evidence of the presence of any cation with higher scattering, in accord with the chemical composition of the crystal (Table 5).

Bond-valence calculations for paranatisite (Table 4) show that O(6) receives only 1.60 valence units (*vu*) in incident bond-valence (for the average structure). Inspection of Table 4 shows that O(6) bonds to *Ti*(2A), *Ti*(2B),  $Na(1) \times 2$  and two  $Na(3)$ . Because of the positional disorder of cations over the *Ti*(2A) and *Ti*(2B) sites, O(6) bonds only to a cation at one of these two sites in any local configuration. Table 6 shows the distribution of local bond-valences around both the *Ti*(2A) and *Ti*(2B) sites. For occupancy of both sites by  $Ti^{4+}$ , the incident bond-valence sums are 4.00 and 2.34 *vu*, respectively. This finding suggests that the *Ti*(2A) site is occupied by Ti, and that the *Ti*(2B) site is occupied by other cations. Consider the bond-valence incident at O(6) where *Ti*(2A) is occupied by  $Ti^{4+}$ :  $\Sigma O(6) = 1.32 [Ti(2A)] + 0.19 \times 2 [Na(1)] + 0.30 + 0.12$  [both from  $Na(3)$ ] = 2.12 *vu*, indicating that O(6) is occupied by  $O^{2-}$  in this local arrangement. With an incident bond-valence sum of 2.44 *vu*, *Ti*(2B) cannot be occupied by

$Ti^{4+}$ . However, the unit formula calculated from the electron-microprobe data (Table 5) indicates that there is significant substitution of  $Fe^{3+}$  and Mn for  $Ti^{4+}$  in this crystal. Is *Ti*(2B) completely occupied by  $Fe^{3+}$  and Mn? The structure was refined with the *Ti*(2B) site-occupancy fixed at the amount of substituent  $Fe^{3+}$  indicated by the unit formula. The refinement converged to an *R* index of 6.6% (compared to 5.1%, Table 1), and there were significant residuals in the electron density around these sites. Thus we may conclude that *Ti*(2B) is not occupied exclusively by  $Fe^{3+}$ . A second cycle of refinement was run with all  $Fe^{3+}$  assigned to *Ti*(2B), along with a variable amount of Ti. The refinement converged to an *R* index of 5.1% and a *Ti*(2B) occupancy of 0.24  $Fe + 0.18(2) Ti$ . If *Ti*(2B) is considered as being occupied by  $Fe^{3+}$ , the incident bond-valence sum (Table 6) at the cation is 2.34 *vu*, and the bond valence incident at O(6) is 0.99 *vu*. The incident bond-valence sum at *Ti*(2B) is still lower than expected, but is more in accord with major occupancy of this site by  $Fe^{3+}$  rather than by  $Ti^{4+}$ . The incident bond-valence sum at O(6) is in accord with local occupancy of O(6) by (OH). Thus the O(6) site is occupied by both O and (OH), depending on the local occupancy of the *Ti*(2A) and *Ti*(2B) sites.

*Structure topology*

In the crystal structure of paranatisite, six distinct polyhedra are linked to form a rather dense framework. It is convenient to describe this structure in terms of sheets of polyhedra perpendicular to the three axes of the orthogonal coordinate system; in paranatisite, there are seven distinct types of sheets of polyhedra.

*The [100] direction:* Four sheets stack along the *a* axis, and three of them are distinct. The first sheet (at  $x \approx 0$ ) consists of  $\{Na(2)O_6\}$  octahedra and  $\{Ti(1)O_5\}$  polyhedra (Fig. 1a). In this sheet,  $\{Na(2)O_6\}$  polyhedra share *trans* vertices to form a chain along [001]. Each  $\{Na(2)O_6\}$  octahedron shares two edges with  $\{Ti(1)O_5\}$  polyhedra, and each  $\{Ti(1)O_5\}$  polyhedron links to four  $\{Na(2)O_6\}$  octahedra through a pair of common edges and through a pair of common vertices. The second sheet (at  $x \approx 0.25$  and 0.75) consists of  $\{Na(1)O_6\}$  octahedra and  $(SiO_4)$  tetrahedra linked through common vertices (Fig. 1b). The third sheet (at  $x \approx 0.50$ ) is composed of  $\{Ti(2)O_5\}$  and  $\{Na(3)O_6\}$  polyhedra (Fig. 1c);  $\{Na(3)O_6\}$  octahedra link through common vertices to form a chain along [010]. Each  $\{Na(3)O_6\}$  octahedron has a face, an edge and a vertex in common with three  $\{Ti(2)O_5\}$  polyhedra.

*The [010] direction:* This direction has a short repeat-distance ( $b = 4.800 \text{ \AA}$ ), and there are only two sheets per repeat. The first sheet (at  $y \approx 0$ ) consists of  $\{Ti(1)O_5\}$  square pyramids,  $\{Na(3)O_6\}$  octahedra and  $(SiO_4)$  tetrahedra (Fig. 2a) linked through common vertices. The  $\{Ti(1)O_5\}$  polyhedra point both up and down. The second sheet (at  $y \approx 0.5$ ) consists of  $\{Na(1)O_6\}$ ,

TABLE 6. LOCAL BOND-VALENCES (*vu*) AROUND *Ti*(2A) =  $Ti^{4+}$  AND *Ti*(2B) (=  $Ti^{4+}$  or  $Fe^{3+}$ )

	<i>Ti</i> (2A)	<i>Ti</i> (2B) <sup>†</sup>	<i>Ti</i> (2B) <sup>†*</sup>
O(2)	0.66 <sup>±2</sup>	0.64 <sup>±2</sup>	0.63 <sup>±2</sup>
O(5)	0.68 <sup>±2</sup>	0.48 <sup>±2</sup>	0.45 <sup>±2</sup>
O(6)	1.32	0.20	0.18
Σ	4.00	2.44	2.34

{*Na*(2)*O*<sub>6</sub>} and {*Ti*(2)*O*<sub>5</sub>} polyhedra (Fig. 2b). Chains of {*Na*(1)*O*<sub>6</sub>} octahedra connect through common edges along [100], and {*Na*(2)*O*<sub>6</sub>} octahedra connect *via* common vertices along [001]. These chains intersect to form four-member clusters. In a cluster, each {*Na*(1)*O*<sub>6</sub>} octahedron shares two edges with two {*Na*(2)*O*<sub>6</sub>} octahedra. The {*Ti*(2)*O*<sub>5</sub>} square pyramids are attached to two {*Na*(1)*O*<sub>6</sub>} octahedra through common edges and to two {*Na*(1)*O*<sub>6</sub>} octahedra through common vertices.

*The [001] direction:* There are four sheets for each *c* unit-cell repeat. The first sheet (at *z* ≈ 0.2 and 0.7) consists of {*Ti*(2)*O*<sub>5</sub>}, {*Na*(2)*O*<sub>6</sub>} and (*SiO*<sub>4</sub>) polyhedra (Fig. 2c) and appears similar to the first sheet perpendicular to [010] (Fig. 2a). It differs from the latter in the polar orientation of {*Ti*(2)*O*<sub>5</sub>} square pyramids. Figure 2d shows a sheet of {*Ti*(1)*O*<sub>5</sub>}, {*Na*(1)*O*<sub>6</sub>} and {*Na*(3)*O*<sub>6</sub>} polyhedra (at *z* ≈ 0.46 and 0.96) in which {*Ti*(1)*O*<sub>5</sub>} pyramids share two edges and two vertices with four {*Na*(1)*O*<sub>6</sub>} octahedra. In this sheet, there are

also two chains of (*NaO*<sub>6</sub>) octahedra: {*Na*(1)*O*<sub>6</sub>} octahedra connect *via* common vertices along [100], and {*Na*(3)*O*<sub>6</sub>} octahedra connect through common edges along [010]. A trimeric cluster of (*NaO*<sub>6</sub>) octahedra forms at the intersection of these two chains, and in this cluster, a central {*Na*(3)*O*<sub>6</sub>} octahedron shares two common faces with adjacent {*Na*(1)*O*<sub>6</sub>} octahedra.

#### THE 4<sup>4</sup> PLANE NET

In the crystal structure of paranatisite, there are three sheets of octahedra or square pyramids and tetrahedra (Figs. 1b, 2a, 2c); such sheets occur as structural fragments in several minerals. Their topology is related to the 4<sup>4</sup> plane net, an array of vertices of valence four, connected by edges (Fig. 3a). Such nets (or graphs) have been used extensively to describe connectivity (or bond topology) in crystal structures (*e.g.*, Wells 1977, Smith 1977, 1978, 1979, Hawthorne 1983, Schindler *et al.*

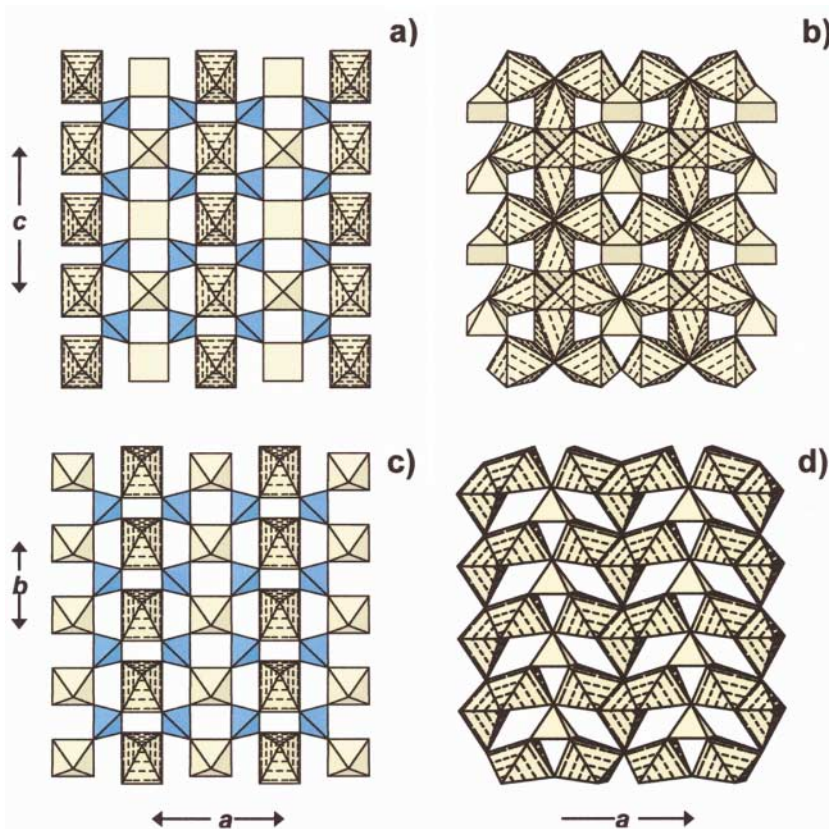


FIG. 2. Four sheets [(010) (a)–(b); (001) (c)–(d)] in the crystal structure of paranatisite: (a) a sheet of *Ti*(1), *Na*(3) and *Si* polyhedra at *y* ≈ 0; (b) a sheet of *Na*(1), *Na*(2) and *Ti*(2) polyhedra at *y* ≈ 0.5; (c) a sheet of *Ti*(2), *Na*(2) and *Si* polyhedra at *z* ≈ 0.2; (d) a sheet of *Ti*(1), *Na*(1) and *Na*(3) polyhedra at *z* ≈ 0.46. Legend as in Figure 1.

1999). The vertices of the graph may represent polyhedra, and the edges of the graph represent the connectivity of the constituent polyhedra. The approach to the topology of crystal structures has concentrated primarily on linkages of tetrahedra. However, one may color the vertices of a graph to represent different types of polyhedra (including vacancies), giving rise to one-colored (Fig. 3a), two-colored (Fig. 3b), three-colored (Figs. 3c, d) and four-colored (Fig. 3e) graphs. In this way, one may examine the topology of crystal structures in which linkage of different types of polyhedra (e.g., tetrahedra and octahedra) is involved. The importance of heteropolyhedral sheets based on the  $4^4$  net in the structure of paranatisite encouraged us to look for

similar sheets in other heteropolyhedral structures. The graphs shown in Figure 3 all have fairly high plane-group symmetry. Many other lower-symmetry graphs are possible, but here we examine only a few high-symmetry representatives, as these describe some of the structures in which we are currently interested.

THE CRYSTAL CHEMISTRY  
OF THE  $[^{6l}M_2^{4l}T_2\phi_{12}]$  SHEET

*Minerals with a  $[^{6l}M_2^{4l}T_2\phi_{12}]$  sheet*

*Sulphohalite*,  $\text{Na}_6 [(\text{SO}_4)_2] \text{F Cl}$ , is a Na sulfate of cubic symmetry (Sakamoto 1968). Its crystal structure

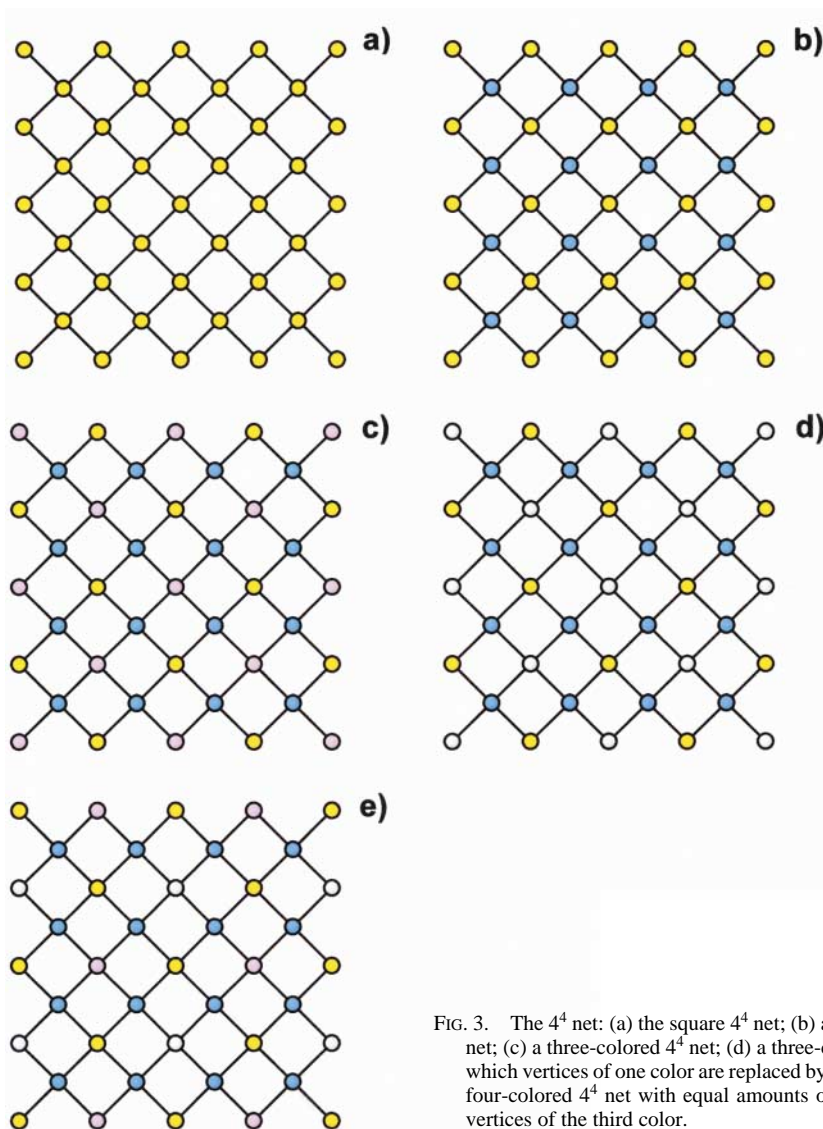


FIG. 3. The  $4^4$  net: (a) the square  $4^4$  net; (b) a two-colored  $4^4$  net; (c) a three-colored  $4^4$  net; (d) a three-colored  $4^4$  net in which vertices of one color are replaced by vacancies; (e) a four-colored  $4^4$  net with equal amounts of vacancies and vertices of the third color.

was recently described by Sokolova & Hawthorne (2001) in terms of trimeric clusters of octahedra. This structure can also be described as a combination of two parallel sheets: (1) a sheet of  $(\text{NaO}_6)$  octahedra at  $z = 0.0$  and  $0.5$ , sharing common vertices, edges and faces, and (2) a sheet of  $(\text{NaO}_6)$  octahedra at  $z = 0.25$  and  $0.75$ , linked to  $(\text{SO}_4)$  tetrahedra through common vertices. As sulphohalite is cubic, these two sheets form two types of framework in the structure. A sheet of  $(\text{Na O}_4 \text{ F Cl})$  octahedra and  $(\text{SO}_4)$  tetrahedra is shown in Figure 4a. This sheet is based on the two-colored  $4^4$  net (Fig. 3b) and can be characterized by a cluster of two octahedra and two tetrahedra:  $[\text{}^{[6]}M_2 \text{}^{[4]}T_2 \phi_{12}]$ , where  $[\text{}^{[6]}M]$  is a [6]-coordinated cation (*i.e.*, Na),  $[\text{}^{[4]}T]$  is a [4]-coordinated cation (*i.e.*, S), and  $\phi$  are anions (*i.e.*, O, F and Cl). In sulphohalite, this cluster has the composition  $[\text{Na}_2 \text{S}_2 \text{O}_{10} \text{F Cl}]^{8-}$  (Table 7).

*Natisite*,  $\text{Na}_2 [\text{Ti O} (\text{SiO}_4)]$ , is a (Na–Ti) orthosilicate and a high-temperature polymorph of  $\text{Na}_2 \text{Ti O} (\text{SiO}_4)$  (Nyman *et al.* 1978). In the crystal structure of natisite,

there is one type of  $[\text{}^{[6]}M_2 \text{}^{[4]}T_2 \phi_{12}]$  sheet of  $(\text{TiO}_5)$  square pyramids and  $(\text{SiO}_4)$  tetrahedra (Fig. 4b), and the pyramids point alternately up and down relative to the plane of the sheet. In the natisite structure, Ti is [5]-coordinated, in contrast to [6]-coordinated Na in sulphohalite, and thus there are two anion vacancies per sheet unit:  $[\text{Ti}_2 \text{Si}_2 \text{O}_{10} \square_2]^4$ . There are several synthetic compounds of the same structure type as natisite; these are listed in Table 7.

*Paranatisite*,  $\text{Na}_4 [\text{Ti O} (\text{Ti,Fe}^{3+}) (\text{O,OH}) (\text{SiO}_4)_2]$ , is characterized by three types of  $[\text{}^{[6]}M_2 \text{}^{[4]}T_2 \phi_{12}]$  sheet. The sheets in Figures 2a and 2c differ from the analogous sheet in natisite (Fig. 4b) in the composition of the *M* sites. In natisite, [5]-coordinated Ti occupies the only one *M* site. In paranatisite, [5]-coordinated Ti and [6]-coordinated Na occupy two *M* sites, and the sheets have the composition  $[\text{Ti Na Si}_2 \text{O}_{10} \square_2]^{10-}$ . The third sheet in the paranatisite structure (Fig. 1b) is similar to the sulphohalite sheet (Fig. 4a), as it contains [6]-coordinated Na and has the composition  $[\text{Na}_2 \text{Si}_2 \text{O}_{10} \square_2]^{7-}$

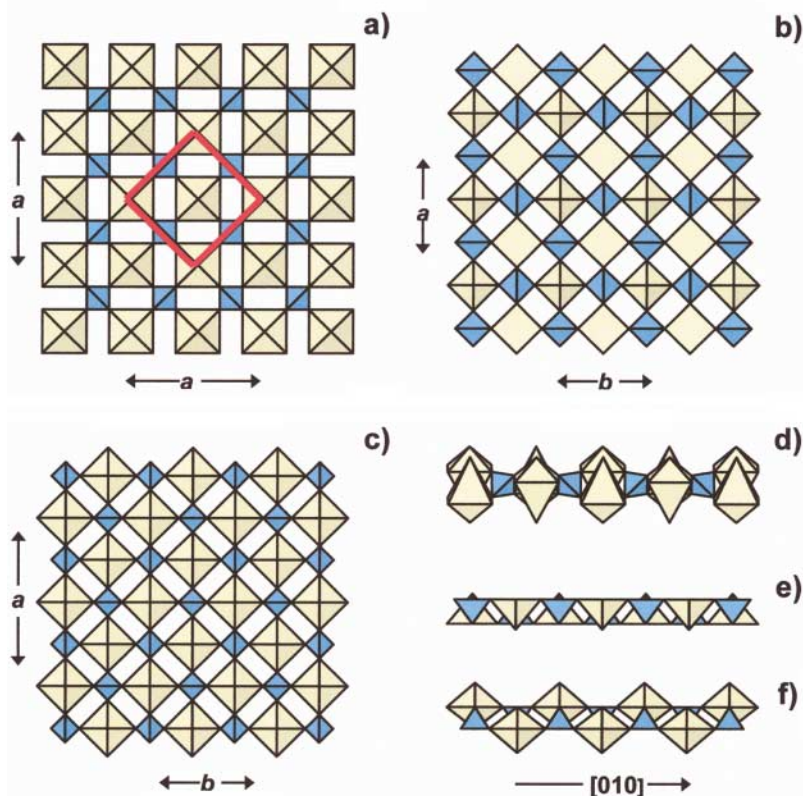


FIG. 4. The  $[\text{}^{[6]}M_2 \text{}^{[4]}T_2 \phi_{12}]$  sheet in the crystal structure of: (a) sulphohalite; red lines indicate the unit  $[\text{Na}_2 \text{S}_2 \text{O}_{10} \text{F Cl}]^{8-}$ ; (b) natisite, and (c) meta-autunite. The  $[\text{}^{[6]}M_2 \text{}^{[4]}T_2 \phi_{12}]$  sheet viewed parallel to the sheet: (d) sulphohalite, (e) natisite, and (f) meta-autunite. Na octahedra (sulphohalite), Ti [5]-coordinated polyhedra (natisite) and U octahedra (meta-autunite) are yellow; S, Si and P tetrahedra are blue.

(Table 7); this sheet is more distorted than the sulphohalite sheet.

*Uranium minerals related to meta-autunite.* Ca [(UO<sub>2</sub>) (PO<sub>4</sub>)<sub>2</sub>] (H<sub>2</sub>O)<sub>6</sub> (Makarov & Ivanov 1960), have been described by Burns *et al.* (1996) and Burns (1999), who showed that the main structural fragment of these structures is a sheet of (U<sup>6+</sup>O<sub>6</sub>) square bipyramids and (PO<sub>4</sub>) or (AsO<sub>4</sub>) tetrahedra. These minerals are meta-uranocircite, Ba [(UO<sub>2</sub>) (PO<sub>4</sub>)<sub>2</sub>] (H<sub>2</sub>O)<sub>6</sub>, threadgoldite, Al [(UO<sub>2</sub>) (PO<sub>4</sub>)<sub>2</sub>] (OH) (H<sub>2</sub>O)<sub>8</sub>, metatorbernite, Cu [(UO<sub>2</sub>) (PO<sub>4</sub>)<sub>2</sub>] (H<sub>2</sub>O)<sub>8</sub>, saléite, Mg [(UO<sub>2</sub>) (PO<sub>4</sub>)<sub>2</sub>] (H<sub>2</sub>O)<sub>10</sub>, abernathyite, K [(UO<sub>2</sub>) (AsO<sub>4</sub>)<sub>2</sub>] (H<sub>2</sub>O)<sub>3</sub>, and metazeunerite, Cu [(UO<sub>2</sub>) (AsO<sub>4</sub>)<sub>2</sub>] (H<sub>2</sub>O)<sub>8</sub> (Table 1). Note that meta-autunite has the same space group (*P4/nmm*) as natBSITE. The U–P sheet in meta-autunite (Fig. 4c) is similar to the Na–S sheet in sulphohalite (Fig. 4a). However, projections in the plane of sheets (Figs. 4d, e, f) show differences in the linkage of octahedra and tetrahedra for sulphohalite and meta-autunite. They also show similar linkage for natBSITE and meta-autunite. Note that the sulphohalite and natBSITE sheets are components of frameworks, whereas the meta-autunite sheet is the structural unit in the seven uranium minerals listed above.

#### Structures with a $[M^{6l} \square^{4l} T_2 \phi_{10} \square_2]$ sheet

We noted above that a three-colored net (Fig. 3c) corresponds to a sheet with three types of cations. If vacancies ( $\square$ ) are regarded as a type of cation, the net is also a three-colored 4<sup>4</sup> net (Fig. 3d) (or a two-colored 8<sup>4</sup> net). A hypothetical sulphohalite-derived sheet based on such a vacancy-containing 4<sup>4</sup> net is shown in Figure 5. Each second octahedron is missing, and the sheet unit is transformed into  $[M^{6l} \square^{4l} T_2 \phi_{10} \square_2]$ . There are several minerals with this type of sheet as a structural fragment: minerals of the garnet group, graphite, girvasite, olmsteadite, johnwalkite, rhomboclase, and gainesite.

*Garnet group:* There are 16 minerals in the garnet group with the general formula  $A_3 B_2 (SiO_4)_3$ , <sup>18</sup>A = Ca, Fe<sup>2+</sup>, Mg and Mn<sup>2+</sup>; <sup>6l</sup>B = Al, Cr<sup>3+</sup>, Fe<sup>3+</sup>, Mn<sup>3+</sup>, Si, Ti, V<sup>3+</sup> and Zr. Spessartine, Mn<sub>3</sub> Al<sub>2</sub> (SiO<sub>4</sub>)<sub>3</sub>, represents this group in Table 7 (Sawada 1999). In the garnet structure, B octahedra and (SiO<sub>4</sub>) tetrahedra form the sheet shown in Figure 6a. The presence of the vacancy in the corresponding 4<sup>4</sup> net allows two of the four (SiO<sub>4</sub>) tetrahedra to rotate around a line connecting the two nearest octahedra. Thus the garnet  $[M^{6l} \square^{4l} T_2 \phi_{10} \square_2]$  sheet is more distorted (*i.e.*, has lower plane-group symmetry) than the  $[^{6l}M_2^{4l} T_2 \phi_{12}]$  sheets in Figures 4a, b and c. In the cubic structure of garnet, three  $[B^{6l} \square^{4l} Si_2 \phi_{10} \square_2]$  sheets intersect each other at right angles to form a framework.

*Graphite.* (Mn<sup>2+</sup>, Ca, Na, Li)<sub>24</sub> Ca<sub>4</sub> Fe<sup>2+</sup><sub>4</sub> Al<sub>8</sub> (PO<sub>4</sub>)<sub>24</sub> F<sub>8</sub> (Rinaldi 1978), has two types of framework: (1) one formed of (AlO<sub>6</sub>) octahedra and (PO<sub>4</sub>) tetrahedra, and (2) one formed of (FeO<sub>6</sub>) octahedra, (CaO<sub>6</sub>F<sub>2</sub>) cubes and (PO<sub>4</sub>) tetrahedra. Here, the first framework is of special

interest as it is formed by three  $[Al^{6l} \square^{4l} P_2 \phi_{10} \square_2]$  sheets similar to the  $[B^{6l} \square^{4l} Si_2 \phi_{10} \square_2]$  sheet in the garnet structure. The  $[Al^{6l} \square^{4l} P_2 \phi_{10} \square_2]$  sheet (Fig. 6b) is topologically identical to the garnet sheet, and differs only in minor rotations of the polyhedra.

*Girvasite.* Na Ca<sub>2</sub> [Mg<sub>3</sub> (OH)<sub>2</sub> (PO<sub>4</sub>)<sub>2</sub> {PO<sub>2</sub> (OH)<sub>2</sub>} (CO<sub>3</sub>)] (H<sub>2</sub>O)<sub>4</sub>, is a good example of an exception to Pauling's (fifth) rule of parsimony (Pauling 1960). The structure of girvasite consists of heteropolyhedral layers parallel to (001) and joined by hydrogen bonds (Sokolova & Egorov-Tismenko 1990). The  $[Mg^{6l} \square^{4l} P_2 \phi_{10} \square_2]$  sheet (Fig. 6c) is the central part of the layer, and is topologically identical to the sheets in garnet and graphite.

*Olmsteadite.* K<sub>2</sub> [Fe<sup>2+</sup><sub>4</sub> Nb<sub>2</sub> O<sub>4</sub> (H<sub>2</sub>O)<sub>4</sub> (PO<sub>4</sub>)<sub>4</sub>] (Moore *et al.* 1976) and *johnwalkite*, K<sub>2</sub> [Mn<sup>2+</sup> Nb O<sub>4</sub> (H<sub>2</sub>O)<sub>4</sub> (PO<sub>4</sub>)<sub>4</sub>] (Dunn *et al.* 1986) were described as phosphates with  $[M^{2+} Nb_2 O_4 (H_2O)_4 (PO_4)_4]^{6-}$  chains. One can also describe these structures in terms of the  $[M^{6l} \square^{4l} T_2 \phi_{10} \square_2]$  sheet:  $[Nb \square P_2 O_{10} \square_2]^{5-}$  (Fig. 6d), in which an (NbO<sub>6</sub>) octahedron shares *cis* vertices with (PO<sub>4</sub>) tetrahedra, in contrast to *trans* vertices in the sheets discussed above. This pattern of sharing results in a pronounced buckling of the sheet in the (001) plane.

*Rhomboclase.* (H<sub>2</sub>O)<sub>2</sub> [Fe (SO<sub>4</sub>)<sub>2</sub> (H<sub>2</sub>O)<sub>2</sub>] (Mereiter 1974), is of special interest here. In its structure, the  $[Fe \square S_2 O_8 (H_2O)_2 \square_2]^{2-}$  sheet consists of (Fe<sup>2+</sup>O<sub>6</sub>) octahedra and (SO<sub>4</sub>) tetrahedra (Fig. 7a); each (FeO<sub>6</sub>) octahedron shares *cis* vertices with two (SO<sub>4</sub>) tetrahedra, with the latter above or below the plane of the sheet (Fig. 7b). The rhomboclase sheet is the most contorted of all the sheets discussed here (Fig. 7c). The synthetic

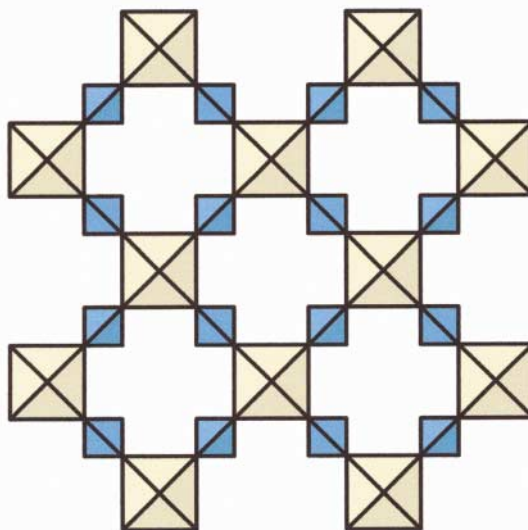


Fig. 5. Hypothetical sheet derived from sulphohalite with a  $[^{6l}M \square^{4l} T_2 \phi_{10} \square_2]$  unit.

TABLE 7. SELECTED MINERALS AND SYNTHETIC COMPOUNDS WITH THE  $[\text{M}_2^{6+}\text{M}_2^{4+}\text{T}_2\phi_{12}]$  SHEET

Mineral	Formula	a (Å)	b (Å)	c (Å)	Sp. gr.	Z	Orientation of sheet(s)	$[\text{M}_2^{6+}\text{M}_2^{4+}\text{T}_2\phi_{12}]$ unit	Ref.
Sulphohalite	$\text{Na}_6[(\text{SO}_3)_2]_2\text{FCl}$	10.150	a	a	<i>Fm</i> 3 <i>m</i>	4	(100)⊙	$\text{O}_2$ [Na Na S <sub>2</sub> ] $\phi_{12}$ $\text{O}_{10}\text{FCij}^{\text{B-}}$	(1)
Nattisite <sup>1</sup>	$\text{Na}_2[\text{TiO}(\text{SiO}_4)]$	6.480	a	5.107	<i>P4</i> 1 <i>nmm</i>	2	(001)	[Ti Ti Si <sub>2</sub> ] $\text{O}_{10}\square_{2}^{\text{A-}}$	(2-5)
Paranattisite <sup>2</sup>	$\text{Na}_4[\text{TiO TiO}(\text{SiO}_4)_2]$	9.181	4.800	9.811	<i>Pmc</i> 21	2	(100)⊙	1[Ti Na Si <sub>2</sub> ] 2[Na Na Si <sub>2</sub> ] $\text{O}_{10}\square_{2}^{\text{A-}}$ $\text{O}_{10}\square_{2}^{\text{B-}}$	(6,7)
Meta-uranocircite <sup>3</sup>	$\text{Ba}[(\text{UO}_2)(\text{PO}_4)_2(\text{H}_2\text{O})_6]$	9.789	9.882	16.868	<i>P2</i> 1 <i>a</i>	4	(001)	[U U P <sub>2</sub> ] $\text{O}_2$ $\text{O}_{12}^{\text{B-}}$	(8)
Threadgoldite <sup>4</sup>	$\text{Al}[(\text{UO}_2)(\text{PO}_4)_2(\text{OH})(\text{H}_2\text{O})_3]$	20.168	9.847	19.719	<i>C2</i> 1 <i>c</i>	8	(100)	[U U P <sub>2</sub> ] $\text{O}_2$ $\text{O}_{12}^{\text{B-}}$	(9)
Metatorbernite	$\text{Cu}[(\text{UO}_2)(\text{PO}_4)_2(\text{H}_2\text{O})_6]$	6.972	a	17.277	<i>P4</i> 1 <i>m</i>	2	(001)	[U U P <sub>2</sub> ] $\text{O}_2$ $\text{O}_{12}^{\text{B-}}$	(10)
Meta-autunite	$\text{Ca}[(\text{UO}_2)(\text{PO}_4)_2(\text{H}_2\text{O})_6]$	6.96	a	8.40	<i>P4</i> 1 <i>nmm</i>	1	(001)	[U U P <sub>2</sub> ] $\text{O}_2$ $\text{O}_{12}^{\text{B-}}$	(11)
Saleeite	$\text{Mg}[(\text{UO}_2)(\text{PO}_4)_2(\text{H}_2\text{O})_{10}]$	6.951	19.947	9.896	<i>P2</i> 1 <i>c</i>	2	(010)	[U U P <sub>2</sub> ] $\text{O}_2$ $\text{O}_{12}^{\text{B-}}$	(12)
Abernathyite <sup>5</sup>	$\text{K}[(\text{UO}_2)(\text{AsO}_4)](\text{H}_2\text{O})_3$	7.176	a	18.126	<i>P4</i> 1 <i>ncc</i>	4	(001)	[U U As <sub>2</sub> ] $\text{O}_2$ $\text{O}_{12}^{\text{B-}}$	(13-17)
Metazeunerite <sup>6</sup>	$\text{Cu}[(\text{UO}_2)(\text{AsO}_4)]_2(\text{H}_2\text{O})_8$	7.105	a	17.704	<i>P4</i> 2 <i>1nmc</i>	2	(001)	[U U As <sub>2</sub> ] $\text{O}_2$ $\text{O}_{12}^{\text{B-}}$	(18,19)
Synthetic comp.	$\text{K}_4[(\text{UO}_2)(\text{PO}_4)_2]$	6.985	a	11.865	<i>P4</i> 2 <i>1nmc</i>	2	(001)	[U U P <sub>2</sub> ] $\text{O}_2$ $\text{O}_{10}\square_{2}^{\text{A-}}$	(20)
Garnet <sup>7</sup>	$\text{Mn}_3[\text{Al}_2(\text{SiO}_4)_3]$	11.650(01)	a	a	<i>Ia</i> 3 <i>d</i>	8	(100)⊙	[Mn □ Si <sub>2</sub> ] $\text{O}_2$ $\text{O}_{10}\square_{2}^{\text{A-}}$	(21)
Griphite	$(\text{Mn}^{2+}\text{CaNaLi})_{24}\text{Ca}_4\text{Fe}^{2+}_4\text{Al}_6(\text{PO}_4)_{24}\text{F}_8$	12.205(8)	a	a	<i>P</i> 3	1	(100)⊙	[Al □ P <sub>2</sub> ] $\text{O}_2$ $\text{O}_{10}\square_{2}^{\text{A-}}$	(22)
Girvasite <sup>8</sup>	$\text{NaCa}_2[\text{Mg}_3(\text{OH})_2(\text{PO}_4)_2(\text{CO}_3)](\text{H}_2\text{O})_4$	6.522(3)	12.25(3)	21.56(2)	<i>P2</i> 1 <i>c</i>	4	(001)	[Mg □ P <sub>2</sub> ] $\text{O}_2$ $\text{O}_9(\text{H}_2\text{O})\square_{2}^{\text{B-}}$	(23)
Olmsteadite	$\text{K}_2[\text{Fe}^{2+}_4\text{Nb}_2\text{O}_4(\text{H}_2\text{O})_4(\text{PO}_4)_4]$	7.512(1)	10.000(3)	6.492(2)	<i>Pb</i> 2 <i>m</i>	1	(100)	[Nb □ P <sub>2</sub> ] $\text{O}_2$ $\text{O}_{10}\square_{2}^{\text{B-}}$	(24)
Johnwalkite	$\text{K}_5[\text{Mn}^{2+}_4\text{Nb}_2\text{O}_4(\text{H}_2\text{O})_4(\text{PO}_4)_4]$	7.516(4)	10.023(8)	6.502(4)	<i>Pb</i> 2 <i>m</i>	1	(100)	[Nb □ P <sub>2</sub> ] $\text{O}_2$ $\text{O}_{10}\square_{2}^{\text{B-}}$	(25)
Rhomboclase <sup>9</sup>	$(\text{H}_5\text{O}_2)[\text{Fe}(\text{SO}_4)_2(\text{H}_2\text{O})_2]$	9.724(4)	18.333(9)	5.421(4)	<i>Pn</i> ma	4	(010)	[Fe □ S <sub>2</sub> ] $\text{O}_2$ $\text{O}_8(\text{H}_2\text{O})_2\square_{2}^{\text{B-}}$	(26,27)
Gaimesite	$\text{Na}_2[\text{ZrBe}(\text{PO}_4)_4]$	6.567(3)	a	17.119(5)	<i>I4</i> 1 <i>amd</i>	2	(001)	[[ZrBe <sub>2</sub> □ <sub>2</sub> ] $\text{O}_2$ $\text{O}_{10}\square_{2}^{\text{B-}}$	(28)

<sup>1</sup> The first structural data on a synthetic analogue of nattisite (2) is quoted. Isostructural synthetic compounds are  $\text{Li}_2\text{TlOSiO}_4$  (3),  $\text{Na}_2\text{TiOGeO}_4$  (4),  $\text{Li}_2\text{VOSiO}_4$  (5).

<sup>2</sup> Isostructural synthetic compound is  $\text{Na}_3(\text{TiO})[\text{SiO}_4]$  (7); <sup>3</sup>  $y = 89.95^\circ$ ; <sup>4</sup>  $\beta = 110.71^\circ$ .

<sup>5</sup> Isostructural synthetic compounds are  $\text{NH}_4[(\text{UO}_2)(\text{AsO}_4)](\text{H}_2\text{O})_3$ ,  $\text{KH}_2\text{O}[(\text{UO}_2)(\text{AsO}_4)]_2(\text{H}_2\text{O})_6$  (13);  $[(\text{UO}_2)\text{H}(\text{PO}_4)](\text{H}_2\text{O})_4$  (14);  $\text{K}[(\text{UO}_2)(\text{PO}_4)](\text{D}_2\text{O})_3$  (15);

$\text{ND}_4[(\text{UO}_2)(\text{PO}_4)](\text{D}_2\text{O})_3$  (16);  $[(\text{UO}_2)\text{D}(\text{AsO}_4)](\text{D}_2\text{O})_4$  (17); <sup>6</sup> Isostructural synthetic compound is  $\text{Li}[(\text{UO}_2)(\text{AsO}_4)]_2(\text{D}_2\text{O})_4$  (19);

<sup>7</sup> As an example, spessartine is given; <sup>8</sup>  $\beta = 89.48(5)^\circ$ ; <sup>9</sup> Isostructural synthetic compound is  $(\text{H}_5\text{O}_2)[\text{In}(\text{SO}_4)_2(\text{H}_2\text{O})_2]$  (27).

⊙ indicates permutation; thus (100)⊙ = (100), (010), (001)

References: (1) Sakamoto (1968); (2) Nyman et al. (1978); (3) Ziadi et al. (1994); (4) Verkhovskii et al. (1970); (5) Rangan et al. (1998); (6) This work; (7) Ziadi et al. (1996); (8) Khosrawan-Sazjed (1992b); (9) Khosrawan-Sazjed (1992b); (10) Stergiov et al. (1993); (11) Makarov & Ivanov (1960); (12) Miller & Taylor (1986); (13) Ross & Evans (1964); (14) Morosin (1978); (15) Fitch & Cole (1991); (16) Fitch et al. (1983); (17) Fitch et al. (1983); (18) Hanic (1960); (19) Fitch et al. (1982); (20) Linde et al. (1980); (21) Sawada (1999); (22) Rinaldi (1978); (23) Sokolova & Egorov-Tismenko (1990); (24) Moore et al. (1976); (25) Dunn et al. (1986); (26) Mereiter (1974); (27) Tudo et al. (1979); (28) Moore et al. (1983).

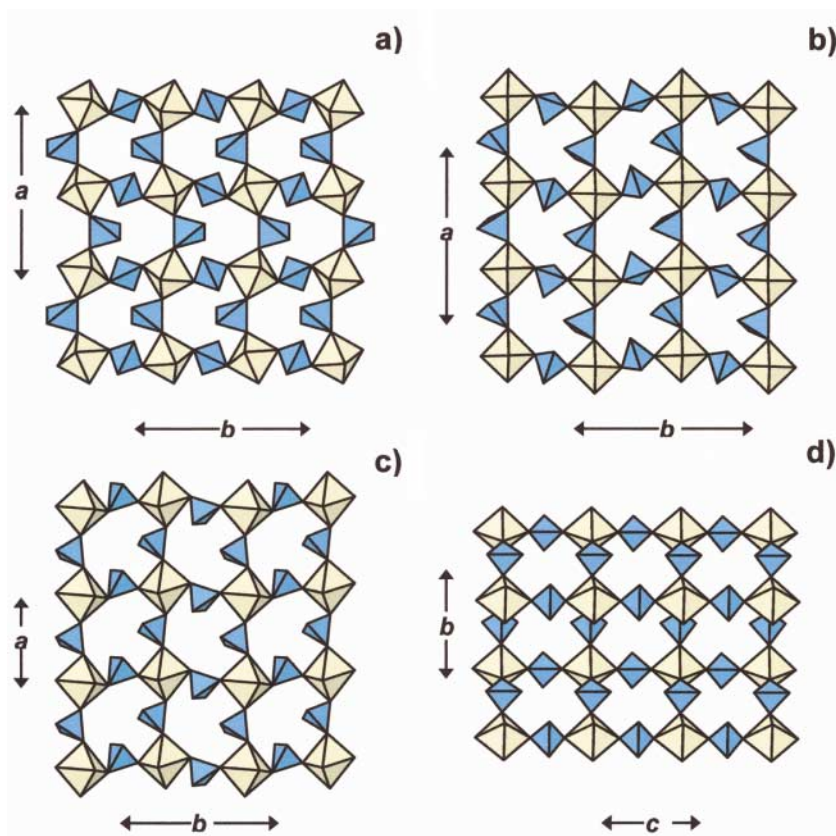


FIG. 6. The  $[{}^6M \square {}^4T_2 \phi_{10} \square_2]$  sheet in the crystal structure of: (a) spessartine, (b) graphite, (c) girvasite, (d) olmsteadite. The Al (spessartine and graphite), Mg (girvasite), and Nb (olmsteadite) octahedra are yellow; Si (spessartine), P (graphite, girvasite, olmsteadite) tetrahedra are blue.

compound  $K_4[(UO_2)(PO_4)_2]$  has a similar sheet (Linde *et al.* 1980).

*Gainesite*, end-member  $Na_2[Zr_2Be(PO_4)_4]$  (Moore *et al.* 1983), is based on an open framework of composition  $[Zr_2BeP_4O_{16}]^{2-}$ . Within this framework, Be and P show major long-range positional disorder. However, the framework must show short-range order if local bond-valence requirements are to be satisfied. The resultant ordered arrangement of a slice through the structure is shown in Figure 8. The corresponding net (Fig. 8a) is intermediate between the nets of Figures 3b and 3d, and the sheet involves alternating  $(BeO_4)$  tetrahedra and vacancies (Fig. 8b), the tetrahedra forming  $[Be(PO_4)_4]$  clusters. According to our scheme, this sheet is of the form  $[(Zr_2Be \square)P_4O_{20} \square_4]^{10-}$  or  $[(ZrBe_{1/2} \square_{1/2})P_2O_{10} \square_2]^{5-}$ . Note that  $M$  now involves a tetrahedrally coordinated cation, Be, and also note that the bond valence of the Be–O bonds,  $\sim 0.50 \nu u$ , is more similar to that of most octahedrally coordinated cations (Na–O to

Al–O are in the range 0.17–0.50  $\nu u$ ) than to that of most tetrahedrally coordinated cations (Si–O to S–O are in the range 1.00–1.50  $\nu u$ ).

#### SUMMARY

Two- and three-dimensional nets are widely used to describe and systematize crystal structures based solely on tetrahedral oxyanions. This approach may also be used to advantage for crystal structures based on polymerization of tetrahedra and octahedra. Thus the  $[{}^6M_2 {}^4T_2 \phi_{12}]$  sheet occurs as a fragment in a wide variety of structures, including silicate, phosphate and sulfate minerals. The recognition of these topological similarities between chemically and paragenetically diverse mineral structures is an important step in the eventual development of structural hierarchies that are based on bond topology (rather than chemical composition).

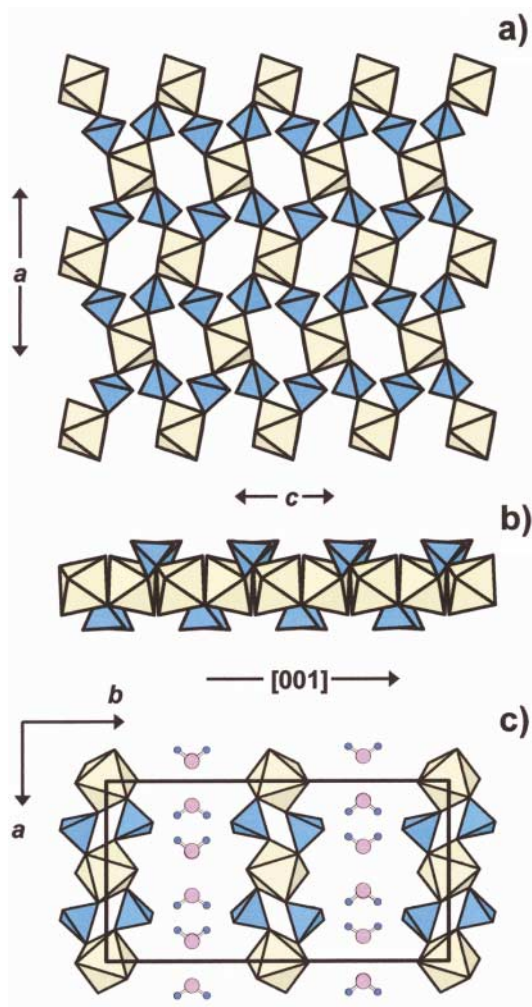


Fig. 7. The crystal structure of rhomboclase: (a) the sheet  $[\text{Fe} \square \text{S}_2 \text{O}_8 (\text{H}_2\text{O})_2 \square]^{2-}$  viewed down [010]; (b) the sheet  $[\text{Fe} \square \text{S}_2 \text{O}_8 (\text{H}_2\text{O})_2 \square]^{2-}$  viewed down [101]; (c) the [001] projection of the crystal structure. The  $(\text{H}_2\text{O})$  groups of the structural unit are omitted for clarity; note that the central H atoms of the interstitial  $(\text{H}_2\text{O})_2$  groups were not located in the refinement, and hence only the terminal  $(\text{H}_2\text{O})$  groups are shown. The  $\text{Fe}^{2+}$  octahedra are yellow, S tetrahedra are blue, interlayer  $(\text{H}_2\text{O})$  groups are shown as pink (O) and purple (H) circles.

#### ACKNOWLEDGEMENTS

We thank Alexander Khomyakov for supplying the paranatisite holotype material, and Andrew Locock, an anonymous reviewer, Associate Editor Peter Burns and the non-sheet-like Bob Martin for their comments on the manuscript. This work was supported by a Canada

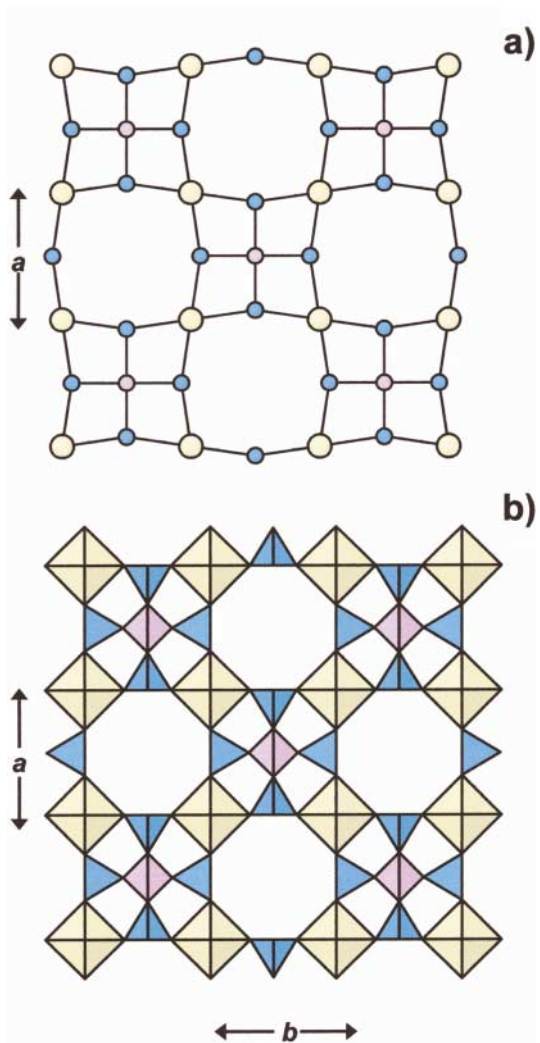


Fig. 8. Gainsite: (a) three-colored net  $4^4$  net; (b) the (001) sheet of Zr octahedra, P and Be tetrahedra. The Zr octahedra are yellow, and P and Be tetrahedra are blue and pink, respectively. The colors of the atoms in the net correspond to colors of the polyhedra in the sheets.

Research Chair in Crystallography and Mineralogy and by Major Equipment and Research Grants from the Natural Sciences and Engineering Research Council of Canada to FCH.

#### REFERENCES

BROWN, I.D. (1981): The bond-valence method: an empirical approach to crystal structure and bonding. *In* Structure and

- Bonding in Crystals II (M. O'Keeffe and A. Navrotsky, eds.). Academic Press, New York, N.Y. (1-30).
- BURNS, P.C. (1999): The crystal chemistry of uranium. In *Uranium: Mineralogy, Geochemistry and the Environment* (P.C. Burns & R. Finch, eds.). *Rev Mineral.* **38**, 37-41.
- \_\_\_\_\_, MILLER, M.L. & EWING, R.C. (1996): U<sup>6+</sup> minerals and inorganic phases: a comparison and hierarchy of crystal structures. *Can. Mineral.* **34**, 845-880.
- CHAO, G.Y. (1985): The crystal structure of gaidonnayite Na<sub>2</sub>ZrSi<sub>3</sub>O<sub>9</sub>•2H<sub>2</sub>O. *Can. Mineral.* **24**, 417-419.
- DUNN, P.J., PEACOR, D.R., STURMAN, D.B., RAMIK, R.A., ROBERTS, W.L. & NELEN J.A. (1986): Johnwalkite, the Mn-analogue of olmsteadite, from South Dakota. *Neues Jahrb. Mineral., Monatsh.*, 115-120.
- FITCH, A.N., BERNARD, L., HOWE, A.T., WRIGHT, A.F. & FENDER, B.E.F. (1983): The room-temperature structure of DUO<sub>2</sub>AsO<sub>4</sub>•4D<sub>2</sub>O by powder neutron diffraction. *Acta Crystallogr.* **C39**, 159-162.
- \_\_\_\_\_, & COLE, M. (1991): The structure of KUO<sub>2</sub>PO<sub>4</sub>•3D<sub>2</sub>O refined from neutron and synchrotron-radiation powder diffraction data. *Mater. Res. Bull.* **26**, 407-414.
- \_\_\_\_\_, & FENDER, B.E.F. (1983): The structure of deuterated ammonium uranyl phosphate trihydrate, ND<sub>4</sub>UO<sub>2</sub>PO<sub>4</sub>•3D<sub>2</sub>O by powder neutron diffraction. *Acta Crystallogr.* **C39**, 162-166.
- \_\_\_\_\_, \_\_\_\_\_ & WRIGHT, A.F. (1982): The structure of deuterated lithium uranyl arsenate tetrahydrate, LiUO<sub>2</sub>AsO<sub>4</sub>•4D<sub>2</sub>O by powder neutron diffraction. *Acta Crystallogr.* **B38**, 1108-1112.
- HANIC, F. (1960): The crystal structure of meta-zeunerite Cu(UO<sub>2</sub>)<sub>2</sub>(AsO<sub>4</sub>)<sub>2</sub>•8H<sub>2</sub>O. *Czech J. Phys.* **10**, 169-181.
- HAWTHORNE, F.C. (1983): Graphical enumeration of polyhedral clusters. *Acta Crystallogr.* **A39**, 724-736.
- IBERS, J.A. & HAMILTON, W.C., eds. (1974): *International Tables for X-ray Crystallography* IV. Kynoch Press, Birmingham, U.K.
- ILYUSHIN, G.D. (1993): New data on the crystal structure of umbite K<sub>2</sub>ZrSi<sub>3</sub>O<sub>9</sub>•H<sub>2</sub>O. *Izv. Akad. Nauk SSSR, Neorg. Mater.* **29**, 971-975 (in Russ.).
- \_\_\_\_\_, KHOMYAKOV, A.P., SHUMYATSKAYA, N.G., VORONKOV, A.A., NEVSKII, N.N., ILYUKHIN, V.V. & BELOV, N.V. (1981a): Crystal structure of a new natural zirconium silicate K<sub>4</sub>Zr<sub>2</sub>Si<sub>6</sub>O<sub>18</sub>(H<sub>2</sub>O)<sub>2</sub>. *Sov. Phys. Dokl.* **26**, 118-120.
- \_\_\_\_\_, VORONKOV, A.A., ILYUKHIN, V.V., NEVSKII, N.N. & BELOV, N.V. (1981b): Crystal structure of natural monoclinic catapleite Na<sub>2</sub>ZrSi<sub>3</sub>O<sub>9</sub>•2H<sub>2</sub>O. *Sov. Phys. Dokl.* **26**, 808-810.
- KHOMYAKOV, A.P., POLEZHAeva, L.I. & SOKOLOVA, E.V. (1992): Paranatisite Na<sub>2</sub>TiSiO<sub>5</sub> – a new mineral. *Zap. Vser. Mineral. Obshchest.* **121**(6), 133-137 (in Russ.).
- KHOSRAWAN-SAZEDJ, F. (1982a): The crystal structure of meta-uranocircite II. Ba(UO<sub>2</sub>)<sub>2</sub>(PO<sub>4</sub>)<sub>2</sub>•6H<sub>2</sub>O. *Tschermaks Mineral. Petrogr. Mitt.* **29**, 193-204.
- \_\_\_\_\_, (1982b): On the space group of threadgoldite. *Tschermaks Mineral. Petrogr. Mitt.* **30**, 111-115.
- LINDE, S.A., GORBUNIVA, Y.E. & LAVROV, A.V. (1980): Crystal structure of K<sub>4</sub>UO<sub>2</sub>(PO<sub>4</sub>)<sub>2</sub> crystals. *Dokl. Akad. Nauk SSSR* **242**, 1083-1085 (in Russ.).
- MAKAROV, YE.S. & IVANOV, V.I. (1960): The crystal structure of meta-autunite, Ca(UO<sub>2</sub>)<sub>2</sub>(PO<sub>4</sub>)<sub>2</sub>•6H<sub>2</sub>O. *Dokl. Acad. Sci. USSR, Earth Sci. Sect.* **132**, 601-603.
- MEREITER, K. (1974): Die Kristallstruktur von Rhomboklas H<sub>5</sub>O<sub>2</sub><sup>+</sup>{Fe[SO<sub>4</sub>]<sub>2</sub>•2H<sub>2</sub>O}<sup>-</sup>. *Tschermaks Mineral. Petrogr. Mitt.* **21**, 216-232.
- MILLER, S.A. & TAYLOR, J.C. (1986): The crystal structure of saleeite, Mg[UO<sub>2</sub>PO<sub>4</sub>]<sub>2</sub>•10H<sub>2</sub>O. *Z. Kristallogr.* **177**, 247-253.
- MOORE, P.B., ARAKI, T., KAMPF, A.R. & STEELE, I.M. (1976): Olmsteadite, K<sub>2</sub>Fe<sup>2+</sup><sub>2</sub>[Fe<sup>2+</sup>(Nb,Ta)<sup>5+</sup><sub>2</sub>O<sub>4</sub>(H<sub>2</sub>O)<sub>4</sub>(PO<sub>4</sub>)<sub>4</sub>], a new species, its crystal structure and relation to vauxite and montgomeryite. *Am. Mineral.* **61**, 5-11.
- \_\_\_\_\_, \_\_\_\_\_, STEELE, I.M., SWIHART, G.H. & KAMPF, A.R. (1983): Gainesite, sodium zirconium beryllophosphate: a new mineral and its crystal structure. *Am. Mineral.* **68**, 1022-1028.
- MOROSIN, B. (1978): Hydrogen uranyl phosphate tetrahydrate, a hydrogen ion solid electrolyte. *Acta Crystallogr.* **B34**, 3732-3734.
- NYMAN, H., O'KEEFFE, M. & BOVIN, J.-O. (1978): Sodium titanium silicate, Na<sub>2</sub>TiSiO<sub>5</sub>. *Acta Crystallogr.* **B34**, 905-906.
- PAULING, L. (1960): *The Nature of the Chemical Bond* (3<sup>rd</sup> ed.). Cornell University Press, Ithaca, N.Y.
- RANGAN, K.K., PIFFARD, Y., JOUBERT, O. & TOURNoux, M. (1998): Li<sub>2</sub>VOSiO<sub>4</sub>: a natisite-type structure. *Acta Crystallogr.* **C54**, 176-177.
- RINALDI, R. (1978): The crystal structure of graphite, a complex phosphate, not a garnetoid. *Bull. Minéral.* **101**, 543-547.
- ROSS, M. & EVANS, H.T., JR. (1964): Studies of torbernite minerals. I. The crystal structure of abernathyite and the structurally related compounds NH<sub>4</sub>(UO<sub>2</sub>AsO<sub>4</sub>)•3H<sub>2</sub>O and K(H<sub>3</sub>O)(UO<sub>2</sub>AsO<sub>4</sub>)<sub>2</sub>•6H<sub>2</sub>O. *Am. Mineral.* **49**, 1578-1602.
- SAKAMOTO, Y. (1968): The size, atomic charges, and motion of the sulfate radical of symmetry 4-3m in the crystal of sulphohalite, Na<sub>6</sub>ClF(SO<sub>4</sub>)<sub>2</sub>. *J. Sci. Hiroshima Univ., Ser. A* **32**, 101-108.
- SAWADA, H. (1999): Electron density study of garnets: Z<sub>3</sub>Al<sub>2</sub>Si<sub>3</sub>O<sub>12</sub> (Z = Mg, Fe, Mn, Ca) and Ca<sub>3</sub>Fe<sub>2</sub>Si<sub>3</sub>O<sub>12</sub>. *J. Solid State Chem.* **142**, 273-278.

- SCHINDLER, M., HAWTHORNE, F.C. & BAUR, W.H. (1999): Metastructures: homeomorphisms between complex inorganic structures and three-dimensional nets. *Acta Crystallogr.* **B55**, 811-829.
- SHELDRIK, G.M. (1997): *SHELXL97, Program for the Solution and Refinement of Crystal Structures*. Univ. of Göttingen, Göttingen, Germany.
- SMITH, J.V. (1977): Enumeration of 4-connected 3-dimensional nets and classification of framework silicates. I. Perpendicular linkages from simple hexagonal net. *Am. Mineral.* **62**, 703-709.
- \_\_\_\_\_ (1978): Enumeration of 4-connected 3-dimensional nets and classification of framework silicates. II. Perpendicular and near-perpendicular linkages from 4.8<sup>2</sup>, 3.12<sup>2</sup> and 4.6.12 nets. *Am. Mineral.* **63**, 960-969.
- \_\_\_\_\_ (1979): Enumeration of 4-connected 3-dimensional nets and classification of framework silicates. III. Combination of helix, and zigzag, crankshaft and saw chains with simple 2D nets. *Am. Mineral.* **64**, 551-562.
- SOKOLOVA, E.V. & EGOROV-TISMENKO, YU.K. (1990): Crystal structure of girvasite. *Sov. Phys. Dokl.* **35**, 308-310.
- \_\_\_\_\_ & HAWTHORNE, F.C. (2001): The crystal chemistry of the [M<sub>3</sub>Φ<sub>11-14</sub>] trimeric structures: from hyperagpaitic complexes to saline lakes. *Can. Mineral.* **39**, 1275-1294.
- \_\_\_\_\_, YAMNOVA, N.A., EGOROV-TISMENKO, YU.K. & KHOMYAKOV, A.P. (1985): Crystal structure of a new mineral Na<sub>8</sub>Ti<sub>3.5</sub>O<sub>2</sub>(OH)<sub>2</sub>[SiO<sub>4</sub>]<sub>4</sub> – a polymorphous modification of natisite. *Sov. Phys. Dokl.* **30**, 822-825.
- STERGIOU, A.C., RENTZEPERIS, P.J. & SKLAVOUNOS, S. (1993): Refinement of the crystal structure of metatorbernite. *Z. Kristallogr.* **205**, 1-7.
- TUDO, J., JOLIBOIS, B., LAPLACE, G., NOWOGROCKI, G. & ABRAHAM, F. (1979): Structure cristalline du sulfate acide d'indium (III) hydraté. *Acta Crystallogr.* **B35**, 1580-1583.
- VERKHOVSKII, V.YA., KUZ'MIN, E.A., ILYUKHIN, V.V. & BELOV, N.V. (1970): Crystal structure of Na titanogermanate Na<sub>2</sub>(TiO)[GeO<sub>4</sub>]. *Sov. Phys. Dokl.* **15**, 7-8.
- WELLS, A.F. (1977): *Three-Dimensional Nets and Polyhedra*. John Wiley and Sons, New York, N.Y.
- ZIADI, A., HILLEBRECHT, H., THIELE, G. & ELOUADI, B. (1996): Crystal structure of orthorhombic LT-Na<sub>2</sub>TiSiO<sub>5</sub> and its relation to the tetragonal HT-form. *J. Solid State Chem.* **123**, 324-330.
- \_\_\_\_\_, THIELE, G. & ELOUADI, B. (1994): The crystal structure of Li<sub>2</sub>TiSiO<sub>5</sub>. *J. Solid State Chem.* **109**, 112-115.

Received October 29, 2001, revised manuscript accepted April xx, 2002.